Mitochondrial matrix copper complex used in metallation of cytochrome oxidase and superoxide dismutase.

Paul A Cobine, Fabien Pierrel, Megan L Bestwick, Dennis R Winge

Mitochondrial matrix copper complex used in metallation of cytochrome oxidase and superoxide dismutase

Paul A. Cobine, Fabien Pierrel, Megan L. Bestwick and Dennis R. Winge*
From the University of Utah Health Sciences Center, Departments of Medicine and Biochemistry, Salt Lake City, Utah 84132
Running title: Mitochondrial copper transport
* Address correspondence to: Dennis Winge, University of Utah Health Sciences Center, Salt Lake City, Utah 84132; Tel: 801-585-5103; Fax: 801-585-5469; Email: dennis.winge@hsc.utah.edu

A mitochondrial matrix copper ligand (CuL) complex, conserved in mammalian cells, is shown for the first time to be the source of copper for cytochrome c oxidase (CcO) and superoxide dismutase-1 (Sod1) within the intermembrane space (IMS) in yeast. Targeting the copper-binding proteins, human Sod1 and Crs5, to the mitochondrial matrix results in growth impairment on non-fermentable medium due to decreased levels of CcO. This effect is reversed by copper supplementation. Matrix-targeted Crs5 diminished Sod1 protein within the IMS and impaired activity of an inner membrane tethered hSod1. Copper binding by the matrix-targeted proteins attenuates levels of the CuL complex without affecting total mitochondrial copper. These data suggest that attenuation of the matrix CuL complex via heterologous competitors limits available copper for metallation of CcO and Sod1 within the IMS. The ligand also exists in the cytoplasm in an apparent metal-free state.

Copper is required within the mitochondrion for assembly of cytochrome *c* oxidase (CcO) and superoxide dismutase (Sod1) (1,2). The copper-binding subunits of CcO are encoded by the mitochondrial genome, so copper insertion into CcO occurs within the organelle. Cox17 functions in Cu(I) delivery within the mitochondrial intermembrane space (IMS) to two accessory proteins, Sco1 and Cox11, for the subsequent copper insertion into CcO (3). Approximately 1-5% of total Sod1 is also localized within the IMS and its localization within this compartment is dependent on Ccs1 (2). Mitochondrial Sod1 is imported as a metal-free polypeptide, so its activation occurs within the IMS by Ccs1 (4). The presence of two copper metalloenzymes that are metallated within the mitochondrion necessitates a specific copper transport pathway to the IMS.

Copper ions enter *Saccharomyces cerevisiae* cells through a combination of high affinity (Ctr1 and Ctr3) and low affinity (Fet4 and Smf1) permeases (5). Within the cytoplasm copper levels are buffered by two metallothioneins (Cup1 and Crs5), that limit the free aqueous copper pool (6). Copper ions are shuttled to sites of utilization by protein-mediated transfer using proteins designated metallochaperones which include Atx1 and Ccs1 (7,8). Atx1 shuttles Cu(I) to the Ccc2 P-type ATPase transporter localized in post-Golgi vesicles for incorporation into the plasma membrane iron permease ferroxidase, Fet3 (9). Ccs1 provides Cu(I) for activation of Sod1 and also catalyzes the formation of an essential disulfide bond in Sod1 (10). Yeast lacking Ccs1 fail to activate Sod1 and have oxygen-dependent phenotypes.

One unknown aspect is how these proteins acquire copper prior to delivery to utilization sites. Metallochaperone function is not impaired in cells lacking the high and low affinity transporters (Ctr1, Ctr3 and Fet4) in replete medium suggesting that the chaperones are not intrinsically dependent on any interaction with these transporters (11).

Cytoplasmic copper ion delivery to Sod1 and Ccc2 is protein-mediated (12). The presence of Ccs1 and Cox17 in both the cytoplasm and IMS made them candidates for shuttling copper ions to the mitochondrion for subsequent functions (13). However, yeast lacking either Ccs1 or Cox17 retain wild type mitochondrial copper levels (14). In addition, tethering Cox17 to the mitochondrial inner membrane by a heterologous membrane-binding domain resulted in its exclusive localization within the organelle, and CcO assembly proceeded normally (15). Thus, Cox17 and Ccs1 cannot be obligate mitochondrial copper transporting metallochaperones. The metallochaperone paradigm predicts that translocation of Cu(I) to the mitochondrion is mediated by another metallochaperone or transport pathway.

Copper is utilized in the metallation of CcO and Sod1 within the IMS, yet the most substantial pool of mitochondrial copper is localized within the matrix (14). The matrix copper pool is present as a soluble, low molecular weight, non-proteinaceous copper-complex (14). Here we show that this copper-complex is conserved in yeast and mouse and that targeting of heterologous copper-binding proteins to the matrix attenuates the activation of both CcO and Sod1 within the IMS. In addition we present data suggesting that the ligand from this copper-complex is found in the cytoplasm where it may recruit, in place of a metallochaperone, the copper that is translocated and stored within the mitochondrial matrix for subsequent use in the IMS for the metallation of CcO and Sod1.

MATERIALS AND METHODS

Yeast strains, culture conditions and standard methods- Yeast strains used in this study were BY4741 (MATa, *leu2*Δ*0*, *met15*Δ*0*, *ura3*Δ*0*, *his3*Δ*1*) and the isogenic *ctr1*Δ*::kanMX4* mutant from Research Genetics (Huntsville, AL). *sod1*Δ KS107 (Mat α*, leu 2-3*, *112*, *his3*Δ*1*, *trp-289a*, *ura3-52*, *sod1*Δ*::TRP1*) was a gift from Dr. V. C. Culotta. All cultures were grown in synthetic defined media with selective amino acids excluded with appropriate filter sterilized carbon source added. Metal concentration were varied by using Bio101 yeast nitrogen base (Q-Bio Gene) plus added 0.1 mM ferrous chloride to give copper deficient conditions. If required, further copper chelation was achieved by adding filter-sterilized copper chelator bathocuproine sulfonate (BCS). Exogenous copper was provided by adding $CuSO_4$ at final concentrations stated. All growth tests were performed at 30^{o}C with 1 in 10 serial dilutions of pre-cultures grown under permissive conditions (e.g. fermentable carbon sources or anaerobic conditions). Anaerobic cultures were prepared in anaerobic jars using BBL GasPak Pd catalysts (Becton, Dickinson and Company, USA).

Vector Constructs- Matrix-targeted human *SOD1* was described previously (14). Matrix-targeted *CRS5* was constructed by adding the coding sequence for the 26 N-terminal amino acids of Sod2 (YHR008C) in-frame to the ORF YOR031W by overlap PCR. A

Myc tag was added to the C-terminus by primer extension. A stop codon present in template genomic DNA (BY4741 background) was corrected to a serine as per previously reported sequence (16) using QuikChange (Stratagene). The fusion sequence construct was cloned into YEp vector with a heterologous *MET25* promoter sequence (300 bp upstream of YLR303W) and a *CYC1* terminator. IM-h*SOD*1 was constructed by inserting the hSod1 ORF in-frame with the sequence encoding the N-terminal 104 residues of Sco2 (YBR024W) that encode a targeting sequence and a transmembrane domain described previously (15). The promoter element was derived from the 200 bp upstream of *SCO1* (YBR037C). All constructs were verified by dideoxynucleotide sequencing prior to use.

Chromotographic fractionations of mitochondria- Mitochondria fractions were prepared as described previously (14). The soluble contents were fractionated as described previously (22). Anionic fractions for reverse phase (RP) HPLC were prepared as above or by adding DEAE (Whatman) resin in batch. The resin was washed with 25 bed volumes of 20 mM ammonium-acetate pH 8.0, and eluted with 5 volumes of 1M ammonium-acetate, pH 8.0. The samples were loaded directly onto a Beckman C18 resin. Unbound fractions were removed with 50 mM ammonium acetate pH 5.0 (or 0.1% TFA to isolate the apo ligand). A 60 min gradient to 100% acetonitrile was used with 1 mL fraction collected. The final fractions were analyzed for copper by flame atomic absorption (Perkin Elmer AAnlyst 100) and for fluorescence in a LB 50 fluorimeter (Perkin Elmer). Excitation and emission scans of copper containing fractions revealed an excitation maximum of 220 nm and emission maximum of 360 nm. Excitation and emission slits of 5 nm were used.

Mouse - Livers from mice were recovered and mitochondria were isolated by mechanical disruption of the tissues by a Potter-Elvehjem homogenizer and differential centrifugation in 0.25 M sucrose followed by gradient purification using a discontinuous 22% over 28% Nycodenz gradient. Integrity and purity were assessed by immunoblotting and enzymatic activity of marker proteins.

Miscellaneous methods - The monoclonal anti-human SOD1 and polyclonal anti-ANT1 and anti-LAMP3 were purchased from Santa Cruz. Yeast Sod1 antisera was a gift from Dr. V.C. Culotta. Antisera to Por1 (porin) and Pgk1 (phosphoglycerol kinase) were from Molecular Probes. Enzyme assays were preformed as described previously (17). Heme was extracted by the pyridine hemochromogen method (18).

RESULTS

Human Sod1 can be activated when targeted to the mitochondrial matrix to complement the oxygen-dependent phenotypes of a *sod2*Δ yeast strain (14). Here we have tested whether expression of matrix-targeted human *SOD1* (m-h*SOD1*) (the matrix targeting sequence of yeast Sod2 was used) has physiological consequences for copper-dependent activities within the mitochondria when compared to cells expressing human *SOD1* lacking the matrix-targeting signal (c-h*SOD1*). Cells lacking Ctr1 were used in these studies as they have diminished copper levels within the cell creating favorable

conditions for the competition experiments. Immunoblotting of *ctr1*Δ transformants demonstrated the presence of the hSod1 proteins in the predicted compartments (Fig. 1A). Both transformants grew equivalently in glucose-containing medium, but the matrix-targeted hSod1 cells were compromised for growth on non-fermentable carbon sources as a result of specific loss of CcO activity (Fig. 1B and data not shown). Respiration-dependent growth was restored by the addition of $CuSO_4$ to the growth medium (Fig. 1B), this correlated with the partial return of CcO activity (data not shown).

The inhibited glycerol growth of m-hSod1 containing cells may arise from hSod1 competition with the matrix CuL complex resulting in decreased availability of copper for the metallation of downstream targets. In fact a catalytically inactive hSod1 containing an R143A substitution was able to exert the same dominant negative phenotype in *ctr1*Δ cells (data not shown). Mitochondrial lysates fractionated by anion exchange chromatography revealed that cells containing m-hSod1 had a diminished level of the matrix CuL complex (fractions 8,9) when compared to mitochondria from control cells with an empty vector (data not shown) or c-hSod1-containing cells (Fig. 1C). An enriched copper fraction now appeared in the column wash fractions (fraction 1-2) that contained m-hSod1 (Fig. 1C inset). Gel filtration chromatography of the wash fractions (Fig. 1D) showed that fractions containing m-hSod1 also contained copper confirming copper binding by m-hSod1.

To assess the specificity of the m-hSod1 competition for matrix copper, a second copper-binding protein was used. The mitochondrial targeting sequence of Sod2 was fused to the cytoplasmic Crs5 copper-metallothionein to generate a matrix-targeted variant (m-Crs5). Immunoblotting showed that the Myc-tagged m-Crs5 was localized in the mitochondrion (Fig. 2A). The presence of Crs5 within the mitochondrial matrix did not impair the growth of yeast on glucose medium (Fig. 2B). However, m-Crs5 compromised growth on glycerol medium, but this inhibitory effect was reversed by the addition of $CuSO_4$ to the growth medium (Fig. 2B). Consistent with this phenotype, CcO activity was impaired in m-Crs5 cells, and the supplementation of $CuSO_4$ to the growth medium restored its activity to a level sufficient to support growth on a non-fermentable carbon source (Fig. 2C). In addition to attenuating CcO activity, the presence of m-Crs5 led to a diminution in the yeast Sod1 protein level within the IMS (Fig. 2D), whereas cytosolic Sod1 was unaffected (data not shown). Sod1 protein level was restored when $CuSO_4$ was added to m-Crs5 cell cultures (Fig. 2D).

The negative effect of matrix Crs5 on IMS Sod1 protein levels was further investigated by engineering a yeast strain containing an IM-tethered hSod1 (via the Sco2 transmembrane domain). Cells lacking endogenous Sod1 were transformed with a vector expressing the IM-h*SOD1* fusion gene. Immunoblotting analysis showed that the fusion protein was intact and exclusively localized in the mitochondrion (Fig. 3A). The IM-hSod1 chimera reversed the oxygen-dependent growth defect and methionine and lysine auxotrophies of *sod1*Δ cells (19) (Fig. 3B). The effect of matrix-targeted Crs5 on IM-hSod1 activity was assessed. The presence of m-Crs5 imparted methionine and lysine

auxotrophies in IM-hSod1-containing cells (Fig. 4A). Both strains grew equivalently in the absence of oxygen. The presence of m-Crs5 reduced the CcO activity (data not shown) and also attenuated the level of the IM-hSod1 chimeric protein (Fig. 4B). Increasing the quantity of $CuSO_4$ in the growth medium significantly reversed the inhibitory effect of m-Crs5 on normoxic growth and CcO activity, but failed to restore the steady state level of IM-hSod1. When IM-hSod1 was expressed from the minimal *MAC1* promoter, protein levels detected by immunoblotting were comparable to those shown in Fig. 4B in cells expressing m-Crs5. This level of expression was sufficient to complement the methionine and lysine auxotrophies (data not shown). Thus, the growth defect observed with m-Crs5 was due to a failure to activate hSod1 and not to decreased levels of IM-hSod1.

Characterization studies were conducted to identify molecular signatures of the matrix CuL complex to enable its quantification. The matrix CuL complex is anionic and low molecular weight (14). Anion exchange fractions of mitochondrial extracts containing the CuL complex were fractionated by reverse-phase HPLC at pH 5 using an acetonitrile gradient (0-100%). A single copper component eluted at 60% of the linear gradient (Fig. 5A). Since aqueous copper is not retained on RP-HPLC, the copper component is ligand bound. The HPLC purified CuL complex was subjected to spectroscopic analysis and was found to fluoresce with excitation and emission maxima at 220 and 360 nm, respectively (Fig. 5B). The quantum yield was enhanced by the addition of potassium cyanide that effectively removes copper from the complex (Fig. 5B). Fluorescence analysis of the HPLC elution fractions revealed a co-fractionation of the 360 nm emission property and copper (Fig. 5A). Upon addition of KCN and re-fractionation by RP-HPLC, the ligand was recovered in a similar column fraction now devoid of copper (data not shown). The emission of the Cu-free ligand was quenched by the addition of Cu(I) but not by Zn(II) or Fe(II) (Fig. 5C). In addition the levels of the anionic fluorescent complex recovered from mitochondrial extracts was increased in cells grown in high exogenous copper that result in increased mitochondrial copper (Fig. 5D). Thus, the anionic ligand concentration correlates with the total mitochondrial copper.

The fluorescence property of the matrix CuL ligand was used to quantify the ligand in mitochondria of *ctr1*Δ cells containing either c-hSod1 or m-hSod1. Clarified mitochondrial lysate from c-hSod1- or m-hSod1-containing cells were adsorbed to an anion exchanger and the total anionic fraction was subsequently applied to reverse phase HPLC at pH 5 (Fig. 5E). Total ligand fluorescence (assessed after cyanide addition) was attenuated in m-hSod1-containing cells. Likewise, mitochondrial ligand fluorescence was attenuated in m-Crs5-containing cells (Fig. 5F). The decreased yield of this fluorescence strongly suggested that this signature of the CuL complex is associated with the source of Cu(I) for CcO and Sod1 metallation within the IMS. The presence of the competitor proteins altered the distribution of the matrix copper without affecting the total mitochondrial copper content.

The fluorescent and chromatographic properties of the ligand

allowed us to address whether the ligand existed in the cytoplasm. The cytosol was fractionated into anionic and uncharged/cationic pools by adsorption on anion exchanger. Anionic components were eluted in a high salt wash of the resin. The column wash and salt eluate were boiled to coagulate proteins. This treatment does not alter the concentration or the chromatographic characteristics of the matrix CuL complex. The clarified fractions were chromatographed by RP-HPLC. Fractions with retention times equivalent to that of the mitochondrial CuL complex were quantified by fluorimetry. The anion exchange salt elution (anionic fraction) contained low levels of the fluorescent adduct, whereas the anion exchange wash showed an abundance of the fluorescent species (Fig. 6A). After treatment with cyanide, this non-anionic fraction appeared to have a quantum yield per cell of nearly eight times over that purified from isolated mitochondria (Fig. 6B). While we cannot eliminate the possibility that at least some of this molecule was liberated from mitochondria by our extraction procedure, the large amount found in these fractions suggests that the ligand is present in the cytoplasm.

The Cu-free molecule present in the cytoplasm could be converted to an anionic Cu adduct by incubation with Cu(I) and DTT (Fig. 6C). The Cu-reconstituted adduct chromatographed equivalently to the anionic CuL complex on reverse phase HPLC. Quantitation of the ligand based on fluorescence revealed that of the total cytoplasmic ligand only around 10% is copper bound (Fig. 6A). Conversely, the ligand found associated with mitochondria is >60% in the anionic Cu-bound form (Fig. 6D). The coordination of copper appears to impart a net negative charge to the complex.

To investigate the conservation of the CuL complex in higher eukaryotes we isolated intact pure mitochondria from mouse liver. The purity of mitochondria was established by western blot analysis and marker enzyme activities (Fig. 7A and not shown). Pure mitochondria were analyzed for total copper content and for heme a+a3 (Fig. 7B). As heme a+a3 is only found in active CcO, the heme a+a3 content can be used to quantify the levels of copper in CcO. The analysis revealed that a range of 10-40% of the copper present in different mitochondrial preparations was associated with active CcO. The mice used in these studies were not matched for age or sex and were from two genetic backgrounds (contributing to the broad range). Therefore as in yeast, CcO does not account for the predominant pool of copper in mouse liver mitochondria.

Soluble mitochondrial extracts were fractionated on anion exchange resin as we had done for yeast mitochondria. The major copper peak was isolated as an anionic complex that was not sensitive to proteases (proteinase K and trypsin) (Fig. 7C). Further fractionation on reverse phase chromatography revealed an identical elution position to the yeast CuL complex (Fig. 7D). The final fraction had the CuL complex fluorescence and the quantum yield was increased by cyanide and quenched by Cu(I), but not by Fe(II) or Zn(II) (Fig. 7E). As in yeast, the ligand from this complex could be isolated in an uncharged state in the cytosol fractions from mouse liver (data not shown). Taken together these data show that the CuL complex is conserved in higher eukaryotes.

DISCUSSION

A matrix CuL complex conserved in the mitochondrion of yeast and mouse liver is shown to be the source of copper for the metallation of CcO and Sod1. In yeast 85% and mouse liver ~70% of the total mitochondrial copper is associated with this matrix Cu-complex. Targeting two different Cu-binding proteins, human Sod1 and Crs5, to the mitochondrial matrix but not the cytoplasm, results in growth impairment on non-fermentable carbon sources due to decreased levels of CcO activity. This effect is reversed by supplementation of $CuSO_4$ to the culture medium. In addition the presence of the matrix targeted Crs5 results in diminished Sod1 protein levels within the IMS and impaired activity of an IM-tethered hSod1. This tethered molecule provided a direct marker of IMS copper. Copper binding by the matrix-targeted proteins attenuates the level of the anionic CuL complex within the matrix without affecting the total mitochondrial copper levels suggesting that biochemical attenuation of the matrix CuL complex via heterologous competitor molecules limits the available copper for redistribution to the IMS for metallation of CcO and Sod1.

Supplementation of cells with exogenous copper leads to an expansion of the matrix Cu(I) pool resulting in an increase in the fluorescent CuL complex (14). Under these conditions, expression of m-hSod1 had a diminished effect on the quantity of the CuL complex. Therefore, the copper reversal of the observed glycerol growth impairment in cells harboring the matrix-targeted proteins likely occurs from the restoration of the matrix CuL pool. The anionic CuL complex is fluorescent and the fluorescence correlates with its copper-binding status. The ligand fluorescence provides a spectroscopic signature that we have used for its quantitation and identification of its presence in the cell cytoplasm. Attempts to identify the ligand using different techniques including MALDI, electrospray and LC mass spectrometry are ongoing. A kinetically labile copper pool within the mitochondria, but not the cytoplasm, was recently confirmed by microprobe x-ray absorption spectroscopy (20).

The ligand is found in the yeast cytoplasm in a largely copper-free state. The cytoplasmic ligand fails to adsorb to an anion exchanger unless it is charged *in vitro* with Cu(I). Cu(I) binding yields an anionic complex that co-fractionates with the matrix Cu(I) complex on RP-HPLC. We postulate that Cu(I) binding to the ligand within the cytoplasm triggers the translocation of the complex to the mitochondrion for storage and subsequent use in CcO and Sod1 metallation within the IMS. The facile expansion of the matrix Cu(I) pool upon supplementation of cells with exogenous copper is consistent with this model and with the high concentration of apo-ligand within the cytoplasm. The model predicts that two types of transporters exist within the mitochondrion. One transporter may function in the translocation of the CuL complex to the matrix compartment and the second transporter is postulated to deliver either Cu(I) or the CuL complex to the IMS for use by Cox17 and Ccs1 for metallation of downstream targets. We are developing genetic strategies to identify the putative transporters. Considering that the ligand is conserved in

mammalian cells, we predict that similar transporters exist in mammalian cells.

The apparent small molecule/metabolite characteristic of the copper ligand described here would be consistent with transport across the mitochondrial inner membrane by the mitochondrial carrier family. This family of 30 proteins has been shown to transport a number of metabolites such a S-adenosyl methionine and thiamine pyrophosphate (21,22). Metal links exist with this family, Mrs3 and Mrs4 are involved in Fe transport for the assembly of Fe-S cluster and heme and Mtm1 has been shown to be involved in Mn/ Fe homeostasis (23-25). The lack of non-fermentable growth phenotypes for other MCF deletion strains suggests that if the putative Cu-transporter required for CcO assembly is a MCF, it may have redundant partners. In the case of yeast Mrs3/4 the iron related phenotypes are much more pronounced in the double deletion strain (26).

The Cu(I) ligand model for copper transport to the mitochondrion, eubacterial in origin, resembles a siderophore strategy of metal ion acquisition by bacteria. Methanotrophic bacteria utilize a Cu-requiring membrane methane monooxygenase in methane catabolism and synthesize the only characterized copper siderophore-like complex, methanobactin. Methanobactin is extruded by methanotrophs into the growth medium when cells are cultured under copper-limiting conditions and is rapidly internalized when copper is provided (27). Methanobactin co-purifies with the particulate methane monooxygenase suggesting that Cu(I)-methanobactin provides copper for the catalytic function of the enzyme. Methanobactin is a small cyclic peptide with two chelating 4-thionyl-5-hydroxyimidazolates that stably binds Cu(I). Similar to the matrix CuL, the fluorescence of methanobactin is quenched by Cu(I). No compelling evidence exists whether the matrix Cu(I) ligand structurally resembles methanobactin. The methanobactin pathway represents a paradigm for how mitochondrial copper acquisition may proceed.

Finally, a number of isolated CcO deficiencies and pleiotrophic loss of respiratory competence with unknown mutations have been found. As our knowledge of the protein mediated assembly and the complex translation and post-translational mechanisms controlling CcO expands, a number of new targets for these mutations will be identified. Unexplained CcO deficiencies in humans may arise from mutations in one of the proposed transporters or mutations that affect the ligand biosynthesis. Importantly, the matrix ligand maintains the cuprous state of copper restricting its potential for generating redox-related damage of mitochondrial components like the mitochondrial DNA. The ability to limit the redox-reactivity may play a role in normal physiology but may also be important in the mitochondrial dysfunction in metal-associated neurodegenerative disorders such ALS and Alzheimer's disease.

Acknowledgements- This work was supported by grant ES03817 from the National Institutes of Health to D.R.W.

References

1. Tsukihara, T., Aoyama, H., Yamashita, E., Tomizaki, T., Yamaguchi, H., Shinzawa-Itoh, K., Hakashima, R., Yaono, R., and Yoshikawa, S. (1995) *Science* **269**, 1069-1074
2. Sturtz, L. A., Diekert, K., Jensen, L. T., Lill, R., and Culotta, V. C. (2001) *J. Biol. Chem.* **276**, 38084-38089
3. Horng, Y. C., Cobine, P. A., Maxfield, A. B., Carr, H. S., and Winge, D. R. (2004) *J. Biol. Chem.* **279**, 35334-35340
4. Field, L. S., Furukawa, Y., O'Halloran, T. V., and Culotta, V. C. (2003) *J. Biol. Chem.* **278**, 28052-28059
5. Puig, S., and Thiele, D. J. (2002) *Curr Opin Chem Biol.* **6**, 171-180
6. Rae, R. D., Schmidt, P. J., Pufahl, R. A., Culotta, V. C., and O'Halloran, T. V. (1999) *Science* **284**, 805-807
7. Huffman, D. L., and O'Halloran, T. V. (2001) *Annu. Rev. Biochem.* **70**, 677-701
8. Field, L. S., Luk, E., and Culotta, V. C. (2002) *J. Bioenerg. Biomembr.* **34**, 373-379
9. Lin, S.-J., Pufahl, R. A., Dancis, A., O'Halloran, T. V. O., and Culotta, V. C. (1997) *J. Biol. Chem.* **272**, 9215-9220
10. Furukawa, Y., Torres, A. S., and O'Halloran, T. V. (2004) *EMBO J.* **23**, 2872-2881
11. Portnoy, M. E., Schmidt, P. J., Rogers, R. S., and Culotta, V. C. (2001) *Mol. Genet. Genomics* **265**, 873-882
12. Huffman, D. L., and O'Halloran, T. V. (2000) *J. Biol. Chem.* **275**, 18611-18614
13. Beers, J., Glerum, D. M., and Tzagoloff, A. (1997) *J. Biol. Chem.* **272**, 33191-33196
14. Cobine, P. A., Ojeda, L. D., Rigby, K. M., and Winge, D. R. (2004) *J. Biol. Chem.* **279**, 14447-14455
15. Maxfield, A. B., Heaton, D. N., and Winge, D. R. (2004) *J. Biol. Chem.* **279**, 5072-5080
16. Culotta, V. C., Howard, W. R., and Liu, X. F. (1994) *J. Biol. Chem.* **269**, 1-8
17. Geller, B. L., and Winge, D. R. (1982) *J. Biol. Chem.* **257**, 8945-8952
18. Berry, E. A., and Trumpower, B. L. (1987) *Anal. Biochem.* **161**, 1-15
19. Slekar, K. H., Kosman, D. J., and Culotta, V. C. (1996) *The Journal of Biological Chemistry* **271**(46), 28831-28836
20. Yang, L., McRae, R., Henary, M. M., Patel, R., Lai, B., Vogt, S., and Fahrni, C. J. (2005) *Proc. Natl. Acad. Sci. USA* **102**, 11179-11184
21. Marobbio, C. M. T., Vozza, A., Harding, M., Bisaccia, F., Palmieri, F., and Walker, J. E. (2002) *EMBO J.* **21**, 5653-5661
22. Marobbio, C. M. T., Agrimi, G., Lasorsa, F. M., and Palamieri, F. (22) *EMBO J.* **22**, 5975-5982
23. Luk, E., Carroll, M., Baker, M., and Culotta, V. C. (2003) *Proc. Natl. Acad. Sci. USA* **100**, 10353-10357

24. Zhang, Y., Lyver, E. R., Knight, S. A. B., Lesuisse, E., and Dancis, A. (2005) *J. Biol. Chem.* **280**, 19794-19807
25. Yang, M., Cobine, P. A., Molik, S., Naranuntarat, A., Lill, R., Winge, D. R., and Culotta, V. C. (2006) *EMBO J.* **epub**
26. Li, F. Y., Nikali, K., Gregan, J., Leibiger, I., Leibiger, B., Schweyen, R., Larsson, C., and Suomalainen, A. (2001) *FEBS Lett.* **494**, 79-84
27. Kim, H. J., Graham, D. W., DiSpirito, A. A., Alterman, M. A., Galeva, N., Larive, C. K., Asunskis, D., and Sherwood, P. M. A. (2004) *Science* **305**, 1612-1615

Figure legends

Fig. 1. Human Sod1 targeted to the mitochondrial matrix has a dominant negative effect on non-fermentable growth. A) Steady-state levels and localization of human Sod1 (hSod1). Mitochondria (M) and cytoplasmic (C) extracts were prepared from *ctr1*Δ cells expressing the mitochondrial matrix-targeted hSod1 (m-hSOD1) or the cytoplasmic hSod1 (c-h*SOD1*). Immunoblotting was with anti-hSod1, anti-Por1 (mitochondrial marker) and anti-Pgk1 (cytoplasmic marker). B) Cells containing high copy vector with m-h*SOD1* or c-h*SOD1* from the *SOD2* promoter were plated at serial dilutions on different carbon sources (2% glucose (top) or 2% glycerol-lactate (middle) or 2% glycerol-lactate plus 0.5 mM $CuSO_4$ added (bottom)). C) Anion exchange profile of soluble extracts from mitochondria of *ctr1*Δ c-hSOD1 (cytoplasmic) or *ctr1*Δ m-hSOD1 (mitochondrial) monitoring total copper in each fraction. The copper profile (fractions 1-20) is displayed for m-hSod1 (solid line) and c-hSod1 (dashed line). The inset is an immunoblot to identify the elution position of hSod1. D) Fractions containing m-hSod1 (or equivalent control from c-hSod1 profile) were separated by size-exclusion chromatography. m-hSod1 was isolated in fractions 10-11 (inset immunoblot) with copper bound (solid line). The equivalent fractions from the c-hSod1 profile showed no copper (dashed line) or hSod1 protein (data not shown). Copper is present in fraction 17, the position that the Cu-complex normally elutes (data not shown) representing a fraction that failed to absorb to the anion exchange column.

Fig. 2. Mitochondrial matrix-targeted Crs5 inhibits non-fermentable growth and causes a decrease in the steady-state levels of IMS localized Sod1. A) Immunoblotting of the mitochondrial (M) and cytoplasmic (C) fractions of *ctr1*Δ cells containing a high copy m-*CRS5*. B) Growth assay of *ctr1*Δ cells containing either empty high copy vector (vec) or with m-*CRS5* plated at serial dilutions on different carbon sources (2% glucose (top), 2% glycerol-lactate (middle) or 2% glycerol-lactate plus 0.5 mM $CuSO_4$ added (bottom)). C) Isolated mitochondria from *ctr1*Δ or *ctr1*Δ m-*CRS5* yeast cells were assayed for CcO activity. D) Immunoblot of isolated mitochondria for the endogenous steady state levels of IMS Sod1.

Fig. 3. Human Sod1 tethered to the inner membrane is fully functional to complement the oxidative stress phenotypes of *sod1*Δ yeast cells. A) Immunoblot of cytoplasm (C) and mitochondria (M) fractions of IM-hSod1-containing *sod1*Δcells. Mitochondrial extracts

of cells expressing the matrix hSod1 were used as a control to show the increased size of the IM-hSod1 fusion. B) Cells grown anaerobically were plated in serial dilution on 2% glucose plates or 2% glucose lacking lysine (Lys-) and methionine (Met-) and grown at normal atmospheric oxygen (Normoxia) or in an anaerobic jar (<0.2% oxygen) (Anoxia) to serve as a loading control.

Fig. 4. IM-h*SOD1* complementation of the lysine and methionine auxotrophies of *sod1*Δ yeast cells can be modulated by the mitochondrial-matrix targeted Crs5. A) *sod1*Δ cells containing the IM-h*SOD1* chimera gene under the control of the *SCO1* promoter and either an empty vector (vec) or the chimeric m-CRS5, were plated in serial dilution on 2% glucose Met- Lys- plates (supplemented with 0.01 mM BCS or $CuSO_4$ as indicated) and grown under normoxia or in an anaerobic jar (Anoxia). B) Steady-state protein levels for m-Crs5 and IM-hSod1. Mitochondria from *sod1*Δ cells expressing IM-h*SOD1* and either an empty vector (vec) or m-*CRS5* were immunoblotted to detect IM-hSod1 and the Myc-tag corresponding to m-Crs5. Two independent mitochondrial preparations are shown.

Fig. 5. Reverse phase purification and characterization of the CuL complex. A) Reverse phase profile of anionic fractions. Fractions (1mL) collected throughout a linear 0-100% acetonitrile gradient (dotted line) were analyzed for copper (bars) and fluorescence (solid line, see panel B). Emissions at 360 nm appear to co-elute with copper. B) The Cu-containing fraction at 60% gradient showed an emission at 360 nm when excited at 220 nm. The quantum yield of 360 nm emissions was enhanced by 1 mM KCN. C) The ligand from the CuL complex was prepared as an apo molecule by RP-HPLC at pH 2.0 then neutralized and emission scan performed. The addition of 0.5 mg copper (+Cu), but not by addition of 0.5 mg of iron and/or zinc (+Fe +Zn), resulted in quenching of the emission. D) Mitochondria from wild-type cells grown with or without 1 mM $CuSO_4$ were lyzed by sonication and the anionic component loaded to RP-HPLC and profile was analyzed for fluorescence. Extracts from cells cultured in medium without added Cu (dashed) versus Cu–supplemented medium (solid) are shown. These conditions result in a 6-fold increase in mitochondrial copper concentration (not shown). E) Soluble, anionic mitochondrial extracts (normalized to mitochondrial protein levels) prepared from *ctr1*Δ m-h*SOD1* or *ctr1*Δ c-h*SOD1* were loaded to RP-HPLC and emission was scanned in all fractions after cyanide treatment. Profiles from cells producing c-hSod1 (dashed) and m-hSod1 (solid) are shown. F) Soluble, anionic mitochondrial extracts were prepared from *sod1*Δ yeast containing IM-h*SOD1* and either an empty vector (vec) or m-*CRS5* RP-HPLC elution profiles, monitoring 360 nm emissions, for vector (dashed) or m-*CRS5* (solid) are shown.

Fig. 6. Quantitation of cytoplasmic and mitochondrial forms of the fluorescent copper ligand. A) A cytoplasmic fraction prepared from WT yeast was subjected to batch anion exchange resin followed by RP-HPLC. All fractions were scanned for fluorescence at 360 nm. Total intensity, corrected for volumes, in fluorescent fractions from the elution of the anion exchange resin (Anionic) or flow through (Non-anionic) is shown. B) Relative mitochondrial and cytoplasmic ligand concentrations were determined in WT by loading soluble extracts of purified mitochondria or cytosol onto RP-HPLC. Final

fractions containing the fluorescent complex were analyzed. C) Cytosolic fraction was treated with copper and dithiothreitol before reapplication to batch anion exchange resin. The copper charged anionic and non-anionic fractions were analyzed on RP-HPLC and total intensity at 360 nm is shown. D) Purified mitochondria from WT yeast were lysed and soluble extracts subjected to batch anion exchange resin followed by RP-HPLC. All fractions were scanned for fluorescence 360 nm. Total intensity of anionic or non-anionic is shown. Error bars represent standard deviation of n>3.

Fig. 7. The copper-complex is found in mouse liver mitochondria. A) Mitochondria were prepared from mouse livers by differential centrifugation and ultracentrifugation on a discontinuous 22%-28% Nycodenz gradient. Immunoblotting of marker enzymes ANT1 (mitochondria) and LAMP3 (lysosome) in crude mitochondria (Cr) versus; the interface (Int) layer (pure intact mitochondria), material that could not enter the 22% Nycodenz layer (<22%) (predominantly lysosome and mitoplasts) and material that pelleted through the 28% layer (>28%) (other membranes) is shown. B) Reduced minus oxidized pyridine hemochromogen spectra of intact mitochondria. The heme a+a3 peak was assessed at 590 nm and a molar extinction coefficient of 26 $mM^{-1}cm^{-1}$ (18) was used to determine the concentration. C) Copper profiles of soluble extracts from purified mitochondria separated by anion exchange. Soluble copper was eluted from the column gradient in a single peak (-PK, solid line). The elution position was not affected by the treatment of the soluble extracts with the proteinase K (+PK, dashed line). D) Soluble, anionic fractions from elution of anion exchange were applied to RP-HPLC at pH 5.0. The fractions from mouse (solid) and yeast (dashed) are shown. E) Emission scans of the fluorescent component after removal of the copper (apo) and after the addition of 0.5 mg copper (+Cu) or 0.5 mg of iron and/or zinc (+Fe (black)) (+Zn (grey)).

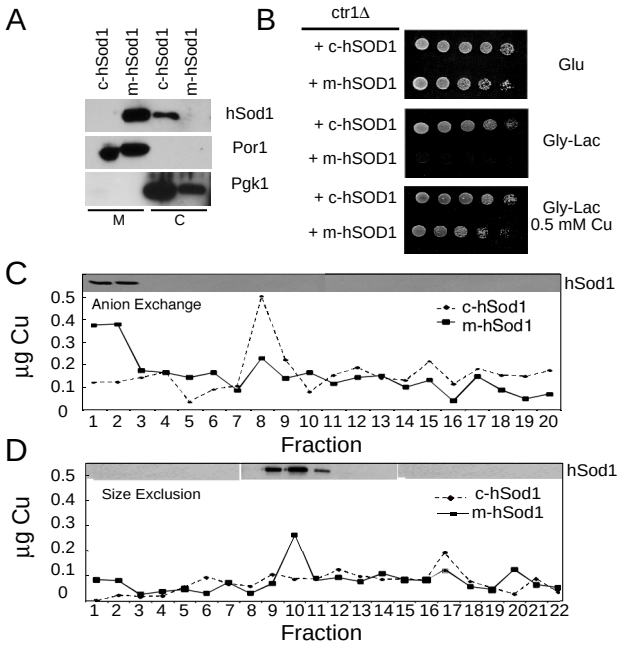
A
c-hSod1
m-hSod1
c-hSod1
m-hSod1
hSod1
Por1
Pgk1
M
C
B
ctr1Δ
+ c-hSOD1
+ m-hSOD1
Glu
+ c-hSOD1
+ m-hSOD1
Gly-Lac
+ c-hSOD1
+ m-hSOD1
Gly-Lac
0.5 mM Cu
C
hSod1
Anion Exchange
c-hSod1
m-hSod1
µg Cu
0.5
0.4
0.3
0.2
0.1
0
1 2 3 4 5 6 7 8 9 10 11 12 13 14 15 16 17 18 19 20
Fraction
D
hSod1
Size Exclusion
c-hSod1
m-hSod1
µg Cu
0.5
0.4
0.3
0.2
0.1
0
1 2 3 4 5 6 7 8 9 10 11 12 13 14 15 16 17 18 19 20 21 22
Fraction

Figure1

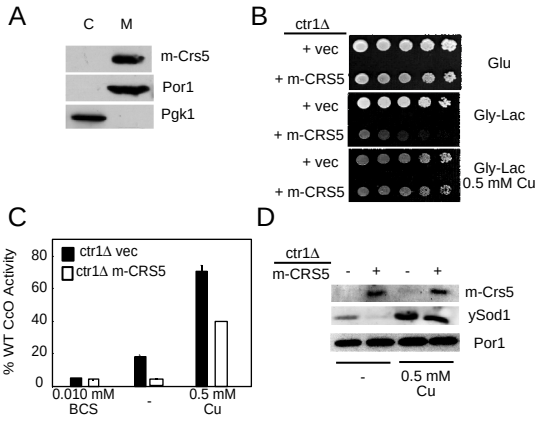
A
C
M
m-Crs5
Por1
Pgk1
B
ctr1Δ
+ vec
+ m-CRS5
Glu
Gly-Lac
Gly-Lac
0.5 mM Cu
C
ctr1Δ vec
ctr1Δ m-CRS5
% WT CcO Activity
0
20
40
60
80
0.010 mM BCS
-
0.5 mM Cu
D
ctr1Δ
m-CRS5
m-Crs5
ySod1
Por1
0.5 mM Cu

Figure 2

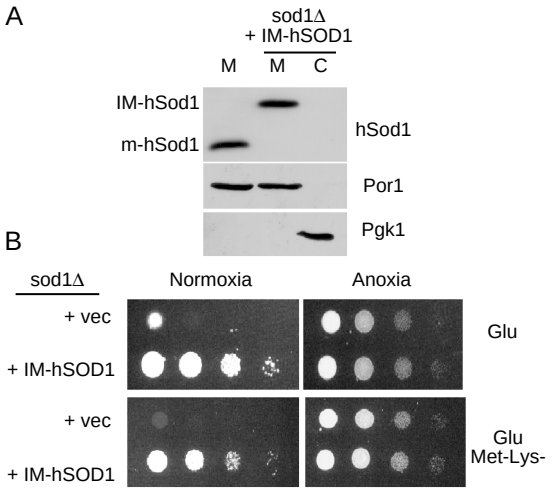
A
sod1Δ
+ IM-hSOD1
M
M
C
IM-hSod1
m-hSod1
hSod1
Por1
Pgk1
B
sod1Δ
Normoxia
Anoxia
+ vec
+ IM-hSOD1
Glu
+ vec
+ IM-hSOD1
Glu
Met-Lys-

Figure 3

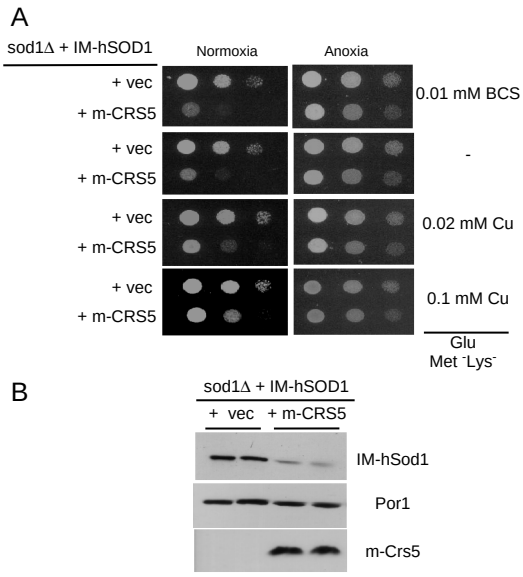
A
sod1Δ + IM-hSOD1
Normoxia
Anoxia
+ vec
+ m-CRS5
0.01 mM BCS
+ vec
+ m-CRS5
-
+ vec
+ m-CRS5
0.02 mM Cu
+ vec
+ m-CRS5
0.1 mM Cu
Glu
Met -Lys-
B
sod1Δ + IM-hSOD1
+ vec
+ m-CRS5
IM-hSod1
Por1
m-Crs5

Figure 4

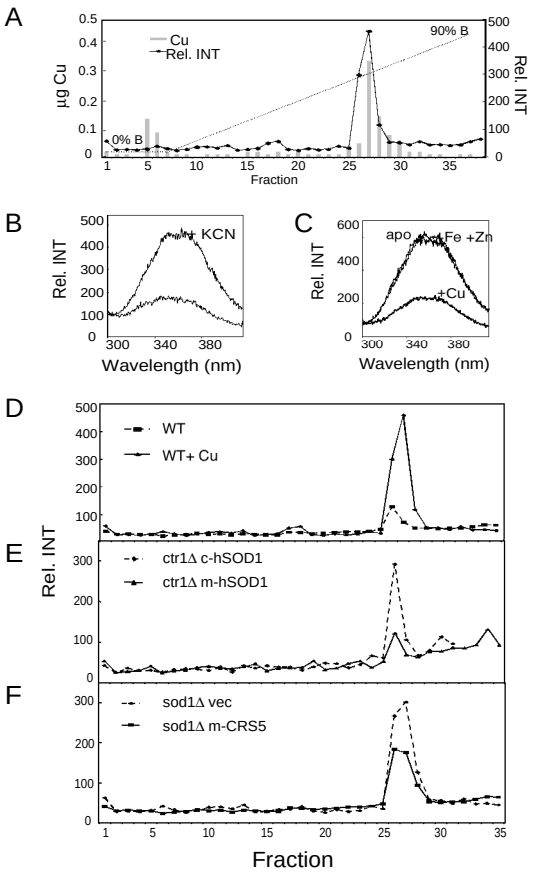
A
Cu
Rel. INT
90% B
0% B
µg Cu
Rel. INT
Fraction
B
+ KCN
Rel. INT
Wavelength (nm)
C
apo
+Fe +Zn
+Cu
Rel. INT
Wavelength (nm)
D
WT
WT+ Cu
E
ctr1Δ c-hSOD1
ctr1Δ m-hSOD1
F
sod1Δ vec
sod1Δ m-CRS5
Rel. INT
Fraction

Figure 5

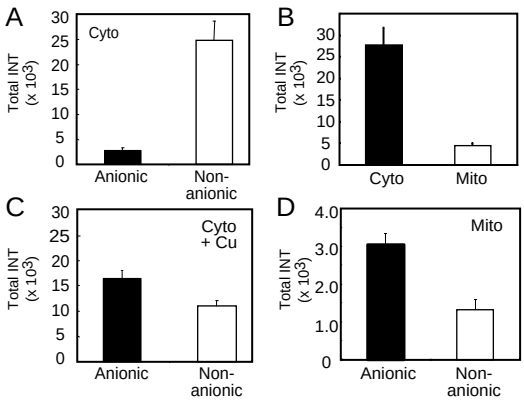
A
Cyto
Total INT (x 10³)
30
25
20
15
10
5
0
Anionic
Non-anionic
B
Cyto
Mito
C
Cyto + Cu
D
Mito
4.0
3.0
2.0
1.0

Figure 6

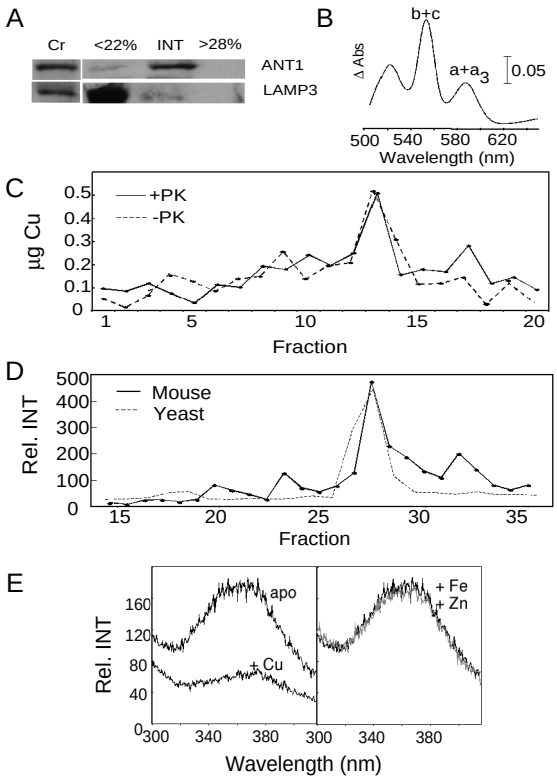
A
Cr
<22%
INT
>28%
ANT1
LAMP3
B
b+c
a+a3
0.05
Δ Abs
500 540 580 620
Wavelength (nm)
C
+PK
-PK
µg Cu
0.5
0.4
0.3
0.2
0.1
0
1 5 10 15 20
Fraction
D
Mouse
Yeast
Rel. INT
500
400
300
200
100
0
15 20 25 30 35
Fraction
E
apo
+ Cu
+ Fe
+ Zn
Rel. INT
160
120
80
40
0
300 340 380 300 340 380
Wavelength (nm)

Figure 7